Elias Sundström[1]
Department of Otolaryngology-Head and Neck Surgery,
University of Cincinnati,
231 Albert Sabin Way,
Cincinnati, OH 45267
e-mail: sundstes@uc.edu

Rehab Talat
Department of Otolaryngology-Head and Neck Surgery,
University of Cincinnati,
231 Albert Sabin Way,
Cincinnati, OH 45267

Ahmad R. Sedaghat
Department of Otolaryngology-Head and Neck Surgery,
University of Cincinnati,
231 Albert Sabin Way,
Cincinnati, OH 45267

Sid Khosla
Department of Otolaryngology-Head and Neck Surgery,
University of Cincinnati,
231 Albert Sabin Way,
Cincinnati, OH 45267

Liran Oren
Department of Otolaryngology-Head and Neck Surgery,
University of Cincinnati,
231 Albert Sabin Way,
Cincinnati, OH 45267

Computational Modeling of Nasal Drug Delivery Using Different Intranasal Corticosteroid Sprays for the Treatment of Eustachian Tube Dysfunction

Eustachian tube dysfunction (ETD) is a common otolaryngologic condition associated with decreased quality of life. The first-line treatment of ETD is intranasal corticosteroid sprays (INCS). Computational fluid dynamics (CFD) was used to study particle deposition on the Eustachian tube (ET) using two commercial INCS (Flonase and Sensimist). Simulations also considered the effects of nostril side, insertion depth, insertion angle, cone spray angle, inhaling rates, wall impingement treatment, and fluid film. Flonase and Sensimist produced different particle size distributions and sizes. Sensimist droplets are smaller, less sensitive to asymmetry in nostrils anatomy and variation in insertion angle, and therefore can reach the posterior nasopharynx more readily. Flonase produces larger particles with greater inertia. Its particles deposition is more sensitive to intrasubject variation in nasal anatomy and insertion angles. The particle deposition on the ET was sensitive to the wall impingement model. The deposition on the ET was insignificant with adherence only <0.15% but increased up to 1–4% when including additional outcomes rebound and splash effects when droplets impact with the wall. The dose redistribution with the fluid film is significant but plays a secondary effect on the ET deposition. Flonase aligned parallel with the hard palate produced 4% deposition efficiency on the ET, but this decreased <0.14% at the higher insertion angle. INCS with larger droplet sizes with a small insertion angle may be more effective at targeting droplet deposition on the ET opening. [DOI: 10.1115/1.4053907]

Keywords: computational fluid dynamics, nasal droplet deposition, spray injection

1 Introduction

Eustachian tube dysfunction (ETD) and its associated morbidities of otitis media with effusion, tympanic membrane retraction, and even cholesteatoma affect an estimated 11 million people per year in the United States [1]. Intranasal corticosteroid sprays (INCS) are considered the first-line treatment for ETD. This treatment aims to deposit droplet particles on the Eustachian tube's (ET) tori tubarii aspect. A previous study has shown that nasal anatomy (such as turbinates and septal deviations) can affect droplet deposition on the ET aspect [2], but the mechanisms of particle deposition were not considered.

In the past decade, computational fluid dynamics (CFD) has evolved into an essential research tool providing high spatiotemporal resolution of nasal airflow and particle deposition in patient-specific airway geometries. It has enabled a physics-based understanding of droplet deposition. CFD has been used extensively in both idealized and patient-specific geometries to study drug delivery performance [3,4]. In the upper airway, numerous studies have investigated the deposition of intranasal sprays in the nasal cavity and paranasal sinuses [3–7]. However, these past CFD studies did not specifically investigate particle deposition on the ET and very few consider variations in the physical properties of different INCS and their respective pump sprays.

Due to the many parameters that may influence the particle deposition from INCS in the nasal cavity, it is crucial to adopt an accurate computational approach with a fast turnaround time. Several studies have employed the Reynolds-averaged Navier–Stokes (RANS) equations with turbulence closure models to govern the transport of the mean flow quantities [8,9]. Li et al. [10] performed systematic numerical assessments comparing different RANS turbulence closure formulations. They found that two-equation models such as K–ω SST can give comparable results of mean flow quantities to more computational expensive large eddy simulation (LES), an approach that is challenging for broad parametric deposition studies [11].

In this study, we use CFD modeling to investigate the deposition of INCS droplets on the ET opening. We simulate the spray from two commercially available INCS, namely, Flonase and Sensimist, to predict particle deposition on the ET in patient-specific models. The INCS nasal position (depth and angle) was also considered. Recent work on nasal spray deposition suggests that agglomerated particles can develop into a liquid fluid film, which in turn can undergo significant translocation to the posterior nasopharynx due to shear force interaction with the airflow and the gravitational force [12]. Similarly, the wall impingement model in this study assumes that particles will stick or adhere upon impact with the mucosal layer in the nasal airway and then subsequently develop a fluid film. One criticism with assuming adherence is that the particle incident Weber number, defined as

[1]Corresponding author.
Contributed by the Materials Division of ASME for publication in the Journal of Engineering and Science in Medical Diagnostics and Therapy. Manuscript received November 22, 2021; final manuscript received February 16, 2022; published online March 11, 2022. Assoc. Editor: Mihai Mihaescu.

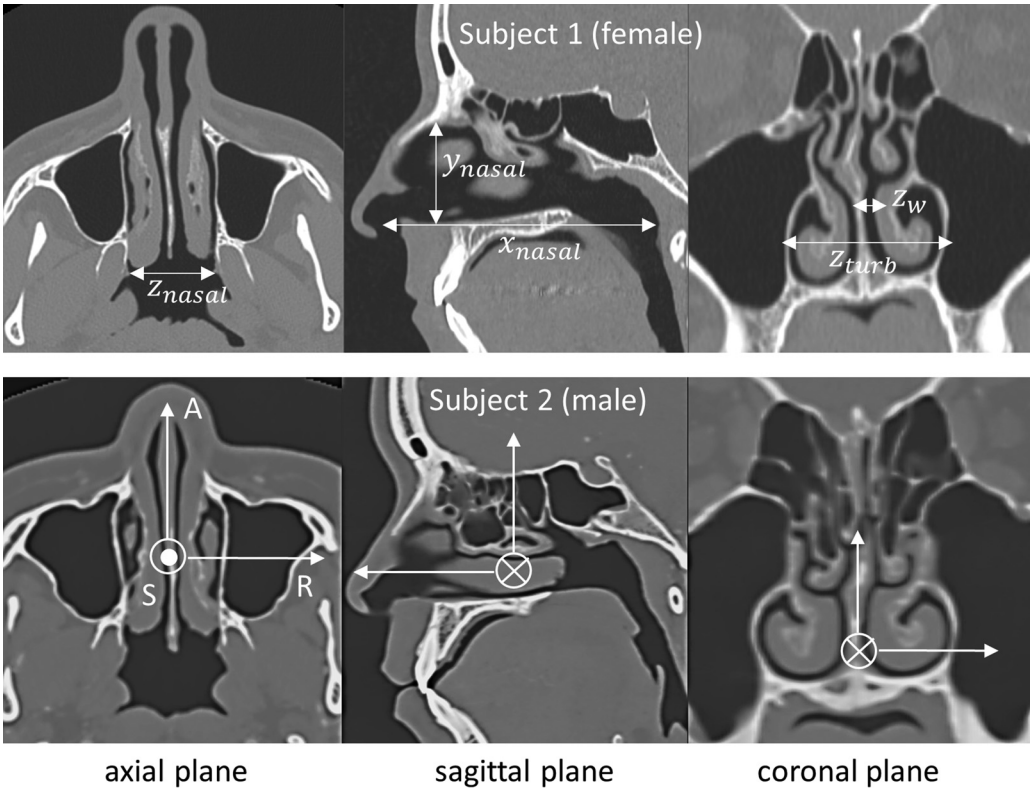

Fig. 1 CT scans of subject 1 (female, top row) and subject 2 (male, bottom row). Axial, sagittal, and coronal planes are shown in the left to right columns. Images from subject 1 are annotated with the different length scales.

$We_I = \rho_P v_{r,n}^2 D_P/\sigma$, must be sufficiently low (less or equal than two). Here, ρ_P—is the particle density, $v_{r,n}$—is the normal component of the particle velocity relative to the wall, D_P—is the particle diameter, and σ—is the surface tension. If the effect of particles with higher incident Weber numbers is not accounted for, it could lead to a significant underestimation of particles reaching the posterior nasopharynx. Therefore, this study also aims to assess the particle deposition efficiency on the ET with the Bai–Gosman wall impingement model that predicts different behavior of liquid particles that impact the mucosal layer of the nasal airway. Specifically, this model attempts to predict how and when particles break up or adhere to the wall [13].

2 Methods

2.1 Model Geometries. Maxillofacial computed tomography (CT) scans were acquired for two subjects. Each CT slice had 0.63-mm thickness with a spatial resolution of 0.43 mm/pixel in each image (Fig. 1). Subjects 1 and 2 were adult female and male, respectively. Both subjects had normal ET function. Demographic information, e.g., age, weight, diagnosis, had been anonymized and the study was deemed exempt by the internal review board at the University of Cincinnati.

The control volume of the nasal airway geometries was delineated from the CT scans using the medical imaging software three-dimensional Slicer [14]. The inlet boundary of the nasal airway was specified externally of the nasal valve (Fig. 2). The outlet was defined at the level of the hypopharynx. All other surfaces of the control volume were specified as no-slip. The length, height, and width of the nasal cavity for both subjects are listed in Table 1. The overall length scales (i.e., x_{nasal}, y_{nasal}, z_{nasal}) show that the subjects have similar nasal airway dimensions.

2.2 Model Parameters. Different constant inhalation flow rates (Q) between 10 and 90 l/min were considered. These values cover the range of normal adult inspiratory flow [15]. The flow was assumed incompressible with a constant air density of 1.2 kg/m^3 and dynamic viscosity of 1.8×10^{-5} Pa·s. A turbulent length scale of 7% to the equivalent diameter and a turbulent intensity of 1% were specified at the inlet.

The CFD model considered the RANS for the incompressible, steady, and viscous flow field [8,16,17]. The K–ω SST model with all $y+$ wall treatment was used for turbulence closure [9,18]. A finite volume upwind scheme of second order was used for discretizing convective and diffusion terms in the governing equations. The segregated flow solver in the CFD software SIMCENTER STAR-CCM+ was used to control the solution coupling of pressure and velocity fields according to the semi-implicit method for pressure linked equations algorithm [8].

The liquid droplets from the INCS were treated as a dispersed phase using the Lagrangian multiphase method [19]. Droplets' transmission and dispersion in the airways were assumed to be affected by turbulence, evaporation, atomization, and droplet break-up. Their drag and shear lift forces were simulated using the Schiller–Naumann correlation and the Sommerfeld correction, respectively. The Ranz–Marshall correlation was used to calculate the Sherwood number for regulation of the droplet evaporation [20]. A primary atomization distribution was assumed at the spray tip with both INCS. Secondary droplet break-up was governed using the Taylor-analogy distortion model with a critical Weber number specified to 12 [21]. The simulations assumed that the droplets remained spherical, had no rotational influence, and had negligible particle-to-particle collision effects. The collision of a droplet with the nasal airway wall was simulated using different wall impingement treatments. These included *adherence* only and *fluid film* treatments. The difference is that liquid droplets merge with the mucosal layer in the nasal airway with the former, while fluid film forms by the droplets deposited on the wall with the latter. The fluid film can subsequently translocate in the airway [12]. Simulations also considered the Bai–Gosman wall impingement treatment [13].

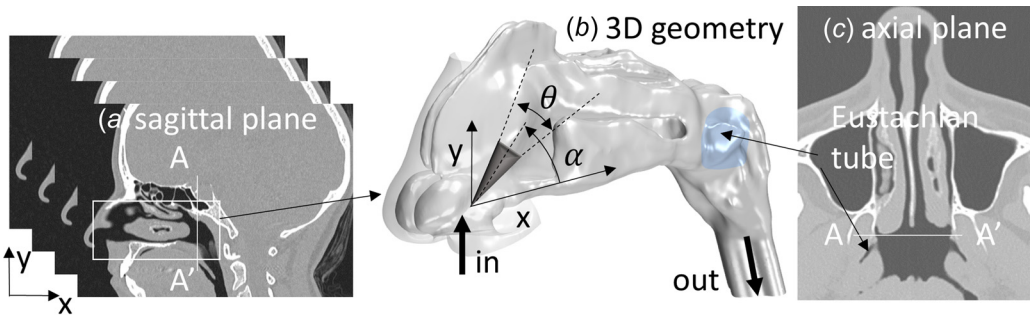

Fig. 2 Reconstruction of the model's control volume geometry based on the CT scans from subject 1. (*a*) Stack of sagittal planes where the red frame highlights the model's geometry region. (*b*) three-dimensional control volume with inlet and outlet boundary conditions annotated with black arrows. The spray cone injector is annotated with a dark gray triangle. The shaded gray area marks the surface used for counting particles depositing on the ET. (*c*) Axial image indicating the location of the ET opening. AA′ is a plane located just upstream of the entrance to the ET and is used for assessing the count of particles that can be deposited into the ET.

Table 1 Nasal geometrical length scales, c.f. Fig. 1 for the location where the length scales are measured

(mm)	Subject 1 (F)	Subject 2 (M)
x_{nasal}	88	88
y_{nasal}	43	40
z_{nasal}	35	33
z_{turb}	29	32
z_w	1.7	1.4

The particle diameter distribution was specified to mimic the characteristics of Flonase and Sensimist. These INCS were investigated by Hosseini et al. [22], and key characteristics used in this study are given in Table 2. Their main difference is a smaller cone angle of 20 deg with the Flonase, which also inject larger sized particles ($d_{p,\text{mean}}$) at a larger standard deviation (σ_p). The droplets were simulated as liquid with a density of 1000 kg/m^3. Both INCS consider a single dose of 0.1 ml during an actuation time of 100 ms at a temperature of 25 °C, corresponding to droplet counts of 1×10^5 and 1×10^6 with the Flonase and Sensimist, respectively. Droplets ejected into the nostrils were in an atomized state, but an explicit primary atomization model was not used anywhere else. The governing equations for the dispersed Lagrangian phase were solved with 2^{15} parcels, where each parcel represents a localized group of droplets having the same properties. The cases with fluid film treatment were simulated unsteady with the time-step size 3×10^{-5} s, resulting in a Courant number around unity.

The INCS nasal position considered three cases for the insertion angle (0 deg, 23 deg, and 43 deg), where $\alpha = 0$ deg was defined as injecting parallel to the hard palate. The nasal position also considered three insertion depths (−5 mm, 0, and +5 mm) where 0 mm was set in the centroid of the nasal vestibule (c.f. Fig. 2).

2.3 Model Verification and Validation. The control volume of the nasal airway model was discretized with polyhedral cells and prismatic cells next to no-slip wall boundaries. The pressure drop between the inlet and the outlet was computed using three

Table 2 Spray cone injector conditions

	Flonase	Sensimist
Outer cone angle, θ (deg)	20	35
Flow rate, Q_p (ml/s)	1.1	1.1
Velocity magnitude (m/s)	14.5	14.4
Droplet distribution (μm)	Normal, $d_{p,\text{mean}} = 126$, $\sigma_p = 45$	Log-normal, $d_{p,\text{mean}} = 57$, $\sigma_p = 33$

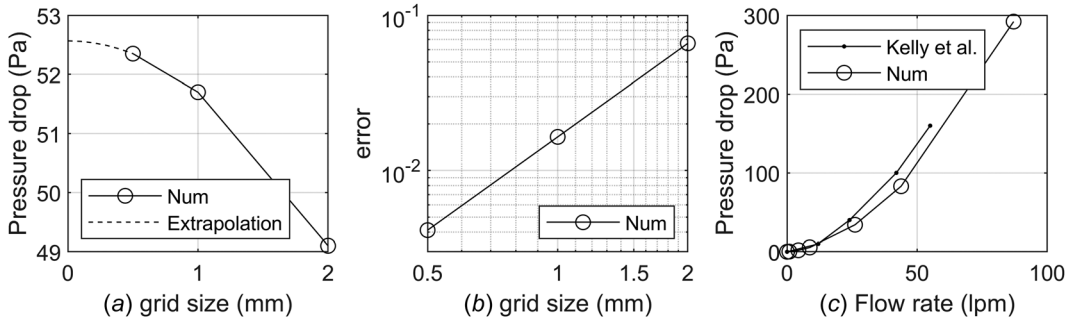

Fig. 3 Grid sensitivity analysis based on fine, medium, and coarse grids. (*a*) Variation of the pressure drop as a function of the grid size. Richardson's second-order extrapolation is shown with a dashed line. (*b*) The numerical error for the infinite grid solution. (*c*) Pressure drop variation as a function of the flow rate. The nasal airway replica measurement from Kelly et al. [23] is included for comparison.

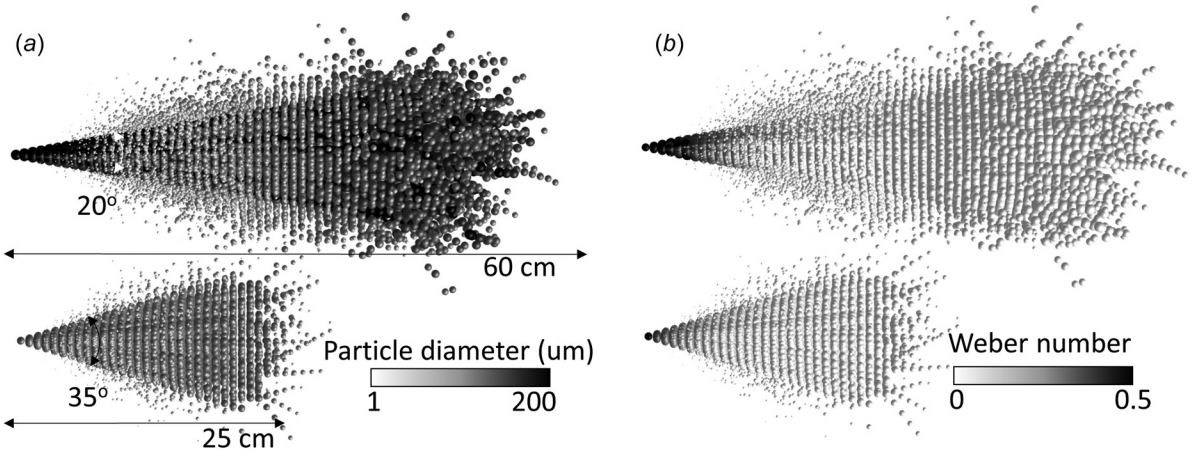

Fig. 4 Penetration length for the Flonase (top) and the Sensimist (bottom). These scatter plots show how far droplet particles would travel from the spray pumps exit outside the airway model under ambient atmospheric conditions. The particles are scaled by the particle diameter and colored by the (*a*) particle diameter and (*b*) Weber number.

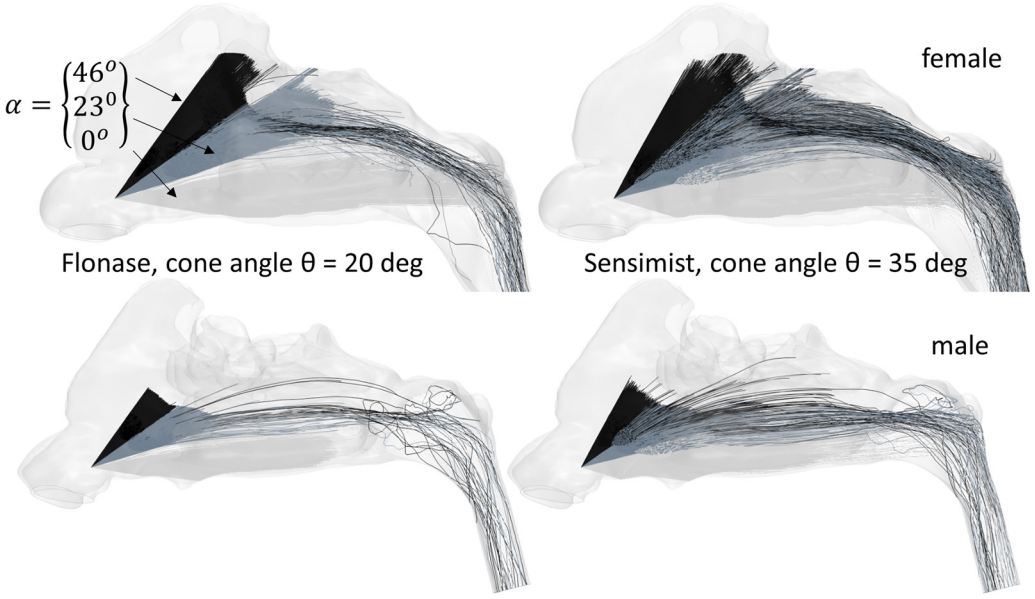

Fig. 5 Particle tracks for three different insertion angles. Flonase to the left and Sensimist to the right. Subject 1 is on the top row and subject 2 is on the bottom row. The inspiratory flow rate is 30 l/min.

different grids (coarse, medium, and fine) (Fig. 3(*a*)). The coarse grid used an averaged cell edge length of 2 mm, the medium grid used 1 mm, and the fine grid used 0.5 mm. Ten prism layers with stretching of 1.5 and thickness of 0.5 mm were used with all grids to yield a wall $y+$ around unity. The finer grid was found to have the least amount of error. Moreover, the error was seen to reduce two orders of magnitude for each grid refinement order (Fig. 3(*b*)). Therefore, the fine grid was used for the subsequent analysis.

Figure 3(*c*) shows the computed pressure drop as a function of the inhalation flow rate. The measurement data from a human nasal airway replica from Kelly et al. [23] are included for comparison. Both the numerical data and the measurement show a nonlinear dependence on the inhalation flow rate.

3 Results

The result section begins with using the simpler adhere wall impingement treatment to assess the effects of different insertion angles (Figs. 5 and 6), the inspiratory flow rates (Fig. 7), and the insertion depth (Fig. 8), and spraying in either nostril (Fig. 9). Next, the effect of using different options for wall treatment is shown (Figs. 10 and 11).

3.1 Effect of Droplet Evaporation. Flonase spray has an overall longer penetration length than the Sensimist spray. Penetration length is defined as the length from the initial spray to when the particle evaporates. Liquid particles steadily lose mass as they are converted into a vapor phase. Therefore, evaporation, and the rate of mass being converted to vapor, is a mechanism that limits how far the particles will travel. When the Flonase is sprayed in the open atmosphere, the simulated penetration length is in the order of 0.5 m and with the Sensimist, it is close to 0.25 m (Fig. 4). These length scales are in good agreement with experimental data by Hosseini et al. [22].

The length scale (x_{nasal}) of the nasal airway is about 88 mm for subjects 1 and 2 (c.f. Table 1), which is 1/3rd of the length scale of evaporation. Therefore, the effect of evaporation in the nasal cavity is considered to be of second-order magnitude.

Figure 4(*b*) shows that the Weber number distribution of the particle scatter is below its critical value for both INCS. Thus, the

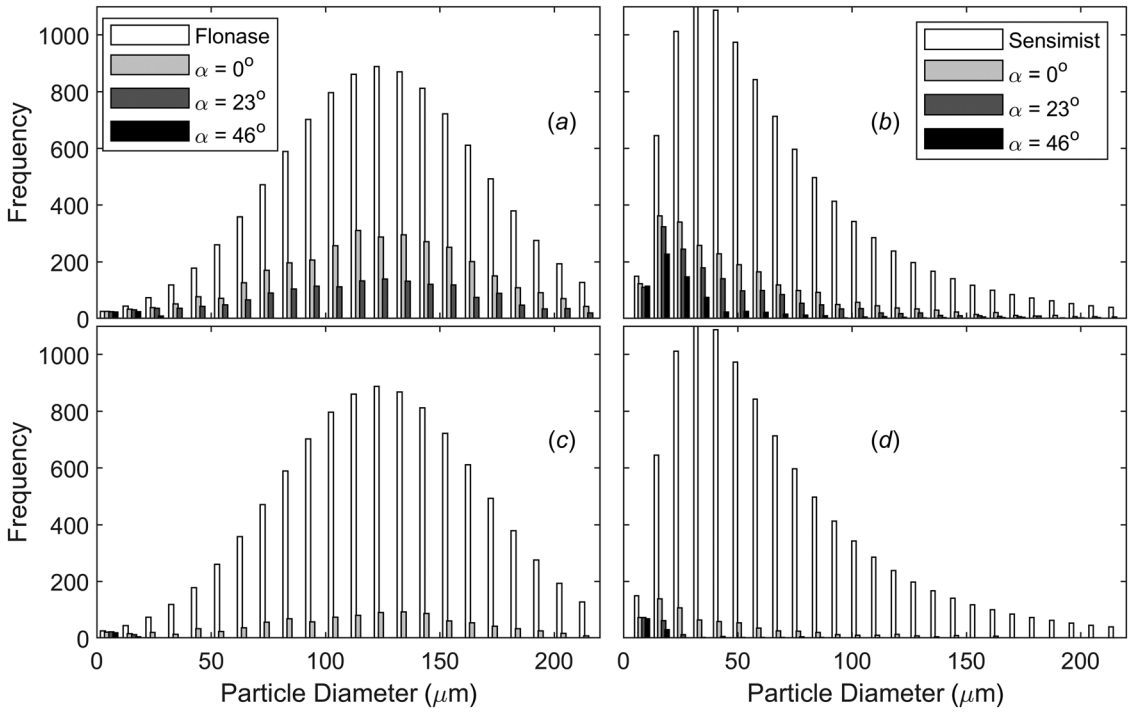

Fig. 6 Particle count (frequency) versus the particle diameter. Distribution is shown for the INCS exit (white bars) and at section AA′ for different insertion angles. Subject 1 is on the top row, and subject 2 is on the bottom row. The Flonase is on the left column and Sensimist to the right.

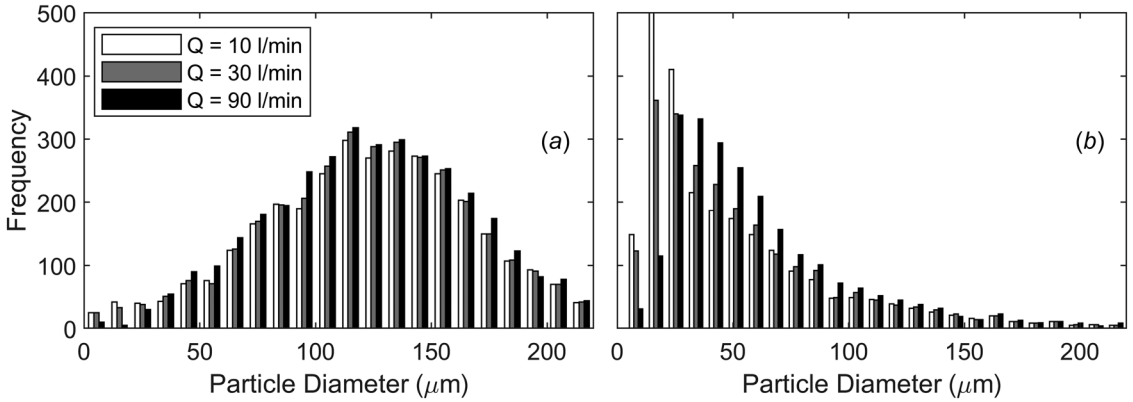

Fig. 7 Particle count (frequency) versus the particle diameter at section AA′ for different inspiratory flow rates. (*a*) Flonase and (*b*) Sensimist.

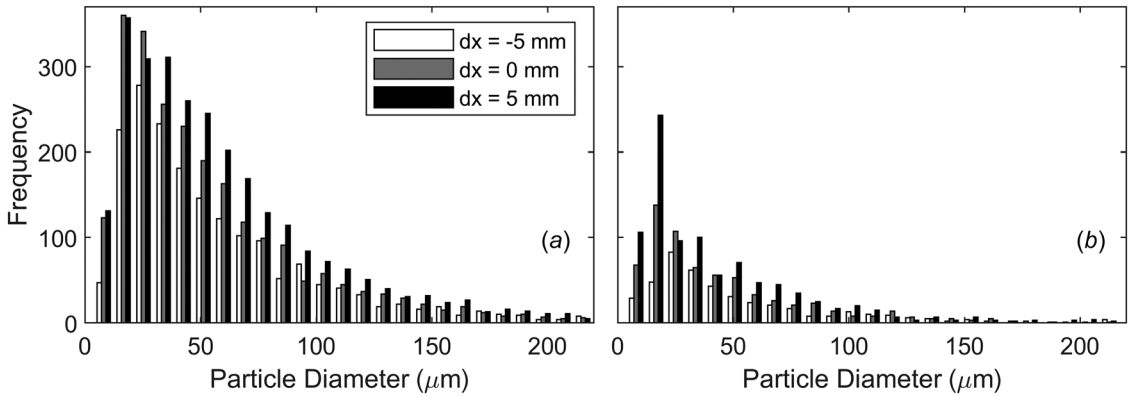

Fig. 8 Particle count (frequency) versus the particle diameter at section AA′ for different insertion depths of the spray injector: (*a*) subject 1 and (*b*) subject 2. All cases are with Sensimist.

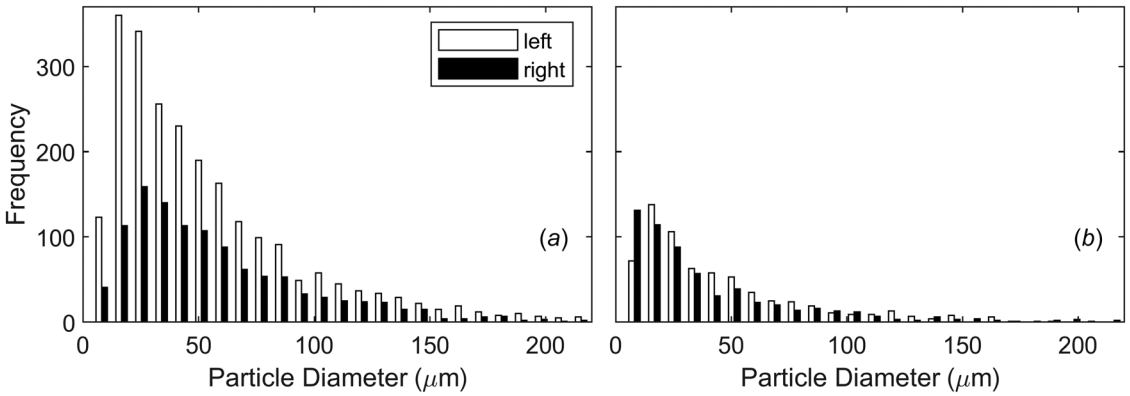

Fig. 9 Difference in particle count (frequency) as a function of particle diameter at section AA' when injecting in each nostril: (*a*) subject 1 and (*b*) subject 2. All cases are with Sensimist.

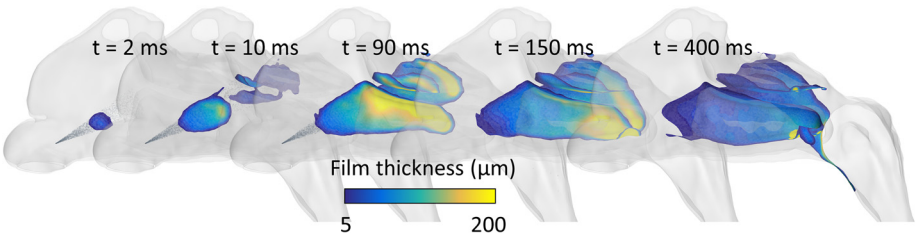

Fig. 10 Fluid film thickness evolution in the nasal airway for subject 1. A dose of 0.1 ml is sprayed using Flonase with injection angle $\alpha = 23$ deg and inspiratory flow rate 30 l/min.

fine spray of particles is considered to be in its atomized state and no further break-up of droplets is expected.

3.2 Effect Intranasal Corticosteroid Sprays Insertion Angle. The insertion angle of the INCS has a significant effect on how droplets are convected in the nasal airway. The difference can be appreciated qualitatively by tracking the particles at three different insertion angles. The baseline case assumes the droplets are injected at $\alpha = 0$ deg, from the x_{nasal} (c.f. Fig. 2(*b*) for the definition of the injection angle α). The other two cases simulate the particles injected at 23 deg, and 46 deg from the baseline. These angles are within the possible administration angle range 0–90 deg suggested by Si et al. [12]. When the spray is injected approximately parallel to the hard palate ($\alpha = 0$ deg), more particle tracks reach the posterior nasal cavity. In both models, the higher the insertion angles, the particle tracks deposit more anteriorly (Fig. 5).

The histogram in Fig. 6 quantifies the particle count at plane AA′ for all considered cases. Plane AA′ is located just upstream of the ET (c.f. Figs. 2(*a*) and 2(*c*)) and can account for all particles passing by the ET entrance. The columns show the particle count at AA′ and compare it with the count at the INCS exit. It shows that Flonase produces larger sized particles with a normal distribution (Figs. 6(*a*) and 6(*c*)).

Independent of the insertion angle, most droplet particles from Flonase are deposited in the nasal cavity before reaching AA′. This can also be appreciated in the particle tracking shown in Fig. 5. The simulation shows that when the spray is injected more parallel to the hard palate, up to 30% of the injected particles in subject 1 (Fig. 6(*a*)) may penetrate posteriorly, whereas with a 23-deg insertion angle, almost all injected particles deposit before reaching the posterior nasal cavity. The deposition efficiency can be defined as the quotient between the number of particles hitting a specific surface (N_{surf}) to the total number of particles injected by the INCS (N_{tot}) as

$$\eta_p = N_{\text{surf}}/N_{\text{tot}} \tag{1}$$

It shows that deposition efficiency was higher for subject 1 than subject 2. In subject 2, only up to 10% of the injected particles may penetrate posteriorly (Fig. 6(*c*)). Thus, the particle deposition efficiency is seen to be sensitive to the patient-specific geometry.

The Sensimist spray produces smaller particle sizes with a log-normal distribution at its exit and smaller particle size variability than Flonase (Figs. 6(*b*) and 6(*d*)). As such, smaller sized particles are also deposited posteriorly. The particles observed at AA′ have a mean particle diameter $d_{p,\text{mean}} = 18\ \mu$m. The particle deposition decreases when the INCS insertion angle is increased. However, Sensimist is seen to be less sensitive to an increase of the insertion angle than Flonase. The quantitative difference in deposition between the two spray pumps is signified by particle inertia. Small inertia indicates that particles can more easily adjust their spatial trajectory to follow the streamlines of the inspiratory airflow. They can, therefore, be carried by the inspiratory airflow around relatively complex and highly curved geometry and reach the posterior regions of the nasal cavity and the nasopharynx. In contrast, the larger Flonase particles with higher inertia are lesser influenced by the inspiratory airflow and deposit more anteriorly, unless the Flonase insertion angle is parallel with the hard palate ($\alpha = 0$ deg).

3.3 Variation Due to Inspiratory Flow Rate. Figure 7 shows the sensitivity of the particle count at section AA′ for variation of the flow rate. It shows that Flonase slightly depends on the inspiratory flow rate, whereas a more significant variation is observed with Sensimist. This variation affects particle sizes with a mean diameter of around 18 μm (c.f. Figs. 6(*c*) and 6(*d*)). For lower inspiratory flow rates, the particle deposition posteriorly increases with Sensimist. Plots are shown only for Subject 1, but similar results were observed for subject 2.

3.4 Effect of Intranasal Corticosteroid Sprays Insertion Depth. Figure 8 shows the variation in particle count at section AA′ based on the insertion depth. The insertion angle was kept at 23 deg and the inspiratory flow rate was held constant at 30 l/min. It shows that deposition in the posterior nasal cavity increases with the Sensimist when the spray tip is further inserted into the nose. This observation is consistent for both subjects.

3.5 Intrasubject Variation Due to Nasal Anatomy. All previous results were based on the INCS injected inside the left nostril of either subject. The effect of spraying in the right nostril was subject-specific (Fig. 9). The data shown are based on the Sensimist injected at 23-deg insertion angle with 30 l/min of inspiratory flow. In subject 1, nearly 50% fewer particles of sizes below 100 μm were observed in section AA′ when spraying inside the right nostril. On the other hand, there was little difference in patient 2 when spraying in either nostril. The difference between subjects probably stems from the asymmetry in the left and right nasal passages, which is more prominent in subject 1.

3.6 Effect of Fluid Film Translocation on the Nasal Airway Wall. The effect of fluid film formation from droplets adhering and agglomerating is shown in Fig. 10. This case considers a dose of 0.1 ml sprayed with Flonase at 23-deg insertion angle and 30 l/min inspiratory flow. The figure shows several instantaneous snapshots with different levels of development and redistribution of the fluid film. In the first snapshot ($t = 2$ ms), the spray has penetrated the nasal passage and a small thin (thickness 5 μm) patch of fluid film is observed. A significant fluid film development occurs until $t = 10$ ms, where the initial patch has grown and a second isolated patch is developing. Toward snapshot $t = 90$ ms, just before the end of the dose administration, the fluid film covers a large area of the middle section of the nasal airway, and the film thickness is now around 200 μm. After the dose administration ($t = 100$ ms), the fluid film mass remains constant and redistributes under the gravitational force and the interaction of shear forces with nasal airflow. The result of this interaction is shown at $t = 150$ ms. The fluid film has redistributed posteriorly and inferiorly toward the soft palate. The fluid film redistribution from $t = 90$ ms until $t = 400$ ms is in the order of a few centimeters per second. This velocity is two orders of magnitude slower than the velocity scale of the liquid droplets (c.f. Table 2). Another interesting observation is that the fluid film redistribution does not pass across the entrance region to the ET, but instead flows more inferiorly, which leads to poor deposition efficiency on the ET.

3.7 Effect of Advanced Wall Impingement Model. In the result shown so far, the wall impingement treatment assumed that the liquid droplets adhere upon collision with the nasal airway wall. If droplet behavior such as rebound and splash is also considered (using the Bai–Gosman wall impingement model), particle distribution changes because of the higher incident Weber number (Fig. 11). With Flonase aligned parallel with the hard palate, almost 75% enters the posterior nasal airway (Fig. 11(*a*)) compared with nearly 55% with Sensimist (Fig. 11(*b*)). These values are higher than the 30% and 20% for the Flonase and Sensismist, respectively, previously predicted. The Flonase shows a reduced particle count at the higher insertion angle, resulting in poor efficiency. Sensimist shows a relatively higher particle count indicating that the insertion angle affects the droplet count at AA′ less.

The simulations also show that only a fraction of the observed particles in the posterior nasal cavity (i.e., AA′ plane) get specifically deposited on the ET. This observation is made by calculating the deposition efficiency (Eq. (1)) on the ET surface. In both subjects, deposition efficiency on the ET was in the order of 1% for both sprays (Fig. 12). These observations are made with the INCS injected in the left nostril at insertion depth $\Delta x = 0$ mm, and inspiratory flow 30 l/min (Fig. 12(*a*)). The adherence-only wall impingement model is even lower (<0.15%). Flonase is sensitive to the insertion angle, with a few percent deposition efficiencies at the smaller insertion angles and almost no efficiency at the larger 46 deg angle. Flonase also shows variability between the two subjects when considering the insertion angle and the insertion depth. Sensimist shows a smaller sensitivity to the insertion angle and between the subjects. Although it has a lower efficiency for insertion angle 0 deg than the Flonase, its efficiency is better at higher insertion angles. Figure 12(*b*) shows that the particle deposition efficiency on the ET consistently increases with the inspiratory flow for all cases. Figure 12(*c*) shows the deposition efficiency with Sensimist increases in both subjects. However, the effect of insertion depth with Flonase was subject-specific. Specifically, the efficiency seemed to vary more and have an optimal insertion depth with subject 1, but it did not change much with subject 2.

4 Discussion

This study showed that particle deposition in the posterior nasal cavity varies with INCS. Specifically, particle deposition at the entrance of the Eustachian tube is more favorable when Flonase is aligned parallel with the hard palate. On the other hand, Sensimist shows less variability in terms of the insertion angle and between the two patient-specific geometries. Varying the inspiratory flow rate, insertion angle, cone angle, or insertion depth does not change the deposition efficiency much. The wall impingement model has a significant effect on the deposition. With adherence, which is commonly used in previous CFD studies on nasal drug delivery, the particle deposition efficiency on the Eustachian tube was below 0.15% in all considered cases. With a more advanced impingement, which includes rebound and splash of the droplets from the wall, the efficiency increases to a few percent. Most particles injected into the nasal cavity will pass by the entrance to the Eustachian tube without being deposited on it. These observations suggest that other spray pumps should be considered when the therapy targets drug delivery to the ET using Flonase or Sensimist.

The deposition mechanism for droplets on the ET remains poorly characterized despite the frequent use of INCS to treat ETD. In this study, we sought to determine the deposition profiles

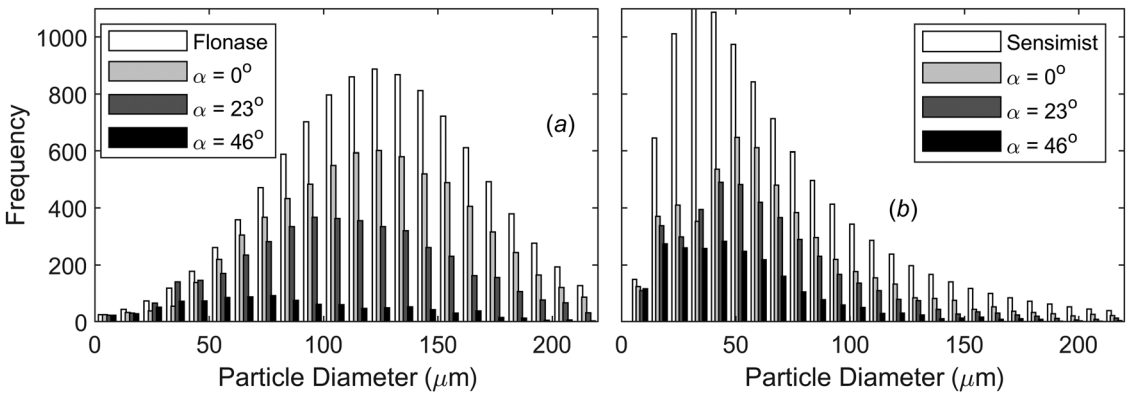

Fig. 11 Particle count (frequency) versus the particle diameter at AA′ for different insertion angles using the Bai–Gosman wall impingement model for subject 1

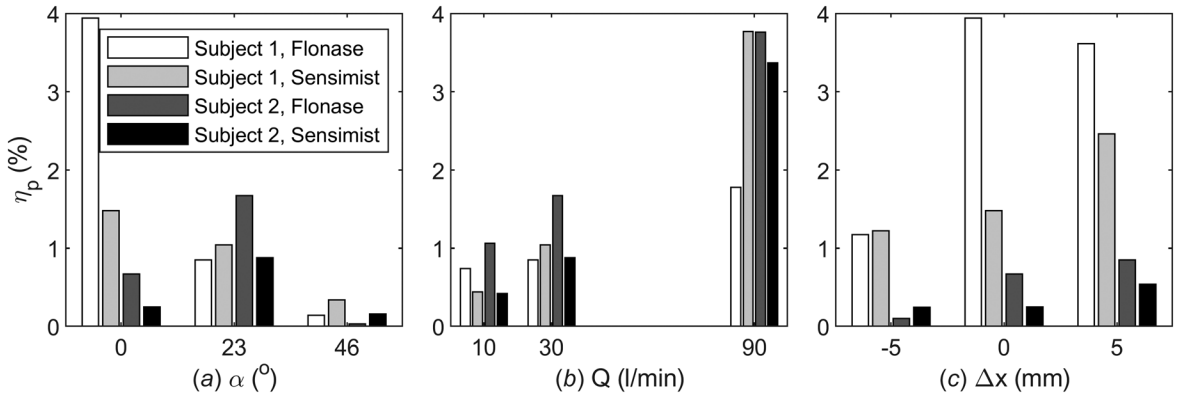

Fig. 12 Particle deposition efficiency at the ET as a function of the (*a*) spray insertion angle. Data is shown for both subjects and the Flonase and Sensimist spray pumps. (*b*) Variation to the flow rate sprayed with insertion angle 23 deg. (*c*) Variation to the insertion depth for Sensimist with insertion angle 0 deg and inspiratory flow 30 l/min.

for patient-specific geometry using two spray pumps that are commercially available for patients. We found that the wall impingement model significantly influences the deposition efficiency of the ET. With a simple adherence impingement model, the deposition efficiency is very low on the ET but increases to a few percent when the Bai-Gosman impingement model was used. We found that Sensimist, with its small particle size and low inertia, shows less variability to the insertion angle that may give an overall higher probability of reaching the posterior nasal cavity and depositing in the nasopharynx than Flonase. However, it was found that a significant number of particles can reach the posterior nasal cavity if the Flonase spray is injected roughly parallel to the hard palate.

Previous studies have often relied on CFD modeling techniques to characterize mechanisms of nasal drug delivery. A major limitation occurs when studies simplify nasal flow parameters to run the CFD simulation. As such, their findings may not accurately represent the mechanisms that exist in vivo, as discussed in the review by Zubair [24]. However, more recent studies have included the patient-specific details of the nasal anatomy, resting breathing rates, and both laminar and turbulent flow. Results can also vary when studies assess different turbulence models with RANS when studying particle deposition in the nasal cavity at resting flow rates [3].

In contrast to previous studies, our study focused on particles depositing on the Eustachian tube and considered the effects of different spray cone angles, insertion angles, inhaling rates, insertion depths, and patient-specific nasal anatomy. Our study also includes the effect of fluid film translocation, which was suggested to affect dose redistribution to the olfactory [12]. It predicted lower deposition efficiency if fluid film develops because of its pathway in the nasal cavity. However, considering the effect of rebound and splash of droplets from the nasal walls predicted a more significant deposition efficiency on the ET than fluid film alone.

The particle Weber number governs the primary atomization and secondary break-up. The Weber number refers to the ratio between inertial forces and surface tension and is defined as the air density times the square of the particle velocity times the particle diameter divided by the surface tension. Primary atomization is the mechanism of forcing a liquid through a narrow orifice at a high pressure that produces an atomized spray of small droplets [25]. Secondary break-up refers to the process of liquid droplets breaking up under the influence of nonuniform surfaces forces that occur in the interaction with the continuous gas phase [26,27]. According to the study by Huh et al. [28], a particle will not undergo the primary atomization stage if the Weber number is less than 12. Moreover, a secondary break-up is also bypassed for subcritical Weber numbers [27], where a Weber number of 12 is critical for a vibrational break-up to manifest. The simulated result showed that the Weber number of the particle cloud with both INCS was less than 12. Hence, it was concluded that the particles are injected in an atomized state with no need for an explicit primary atomization model.

4.1 Study Limitations. Using a small cohort is a limitation that was needed to reduce the number of unknown geometric factors that may influence the result. Examining intra- and intersubject variability in further detail will require are larger cohort. We also used the RANS equations in our CFD modeling, and a future study could benefit from comparing with data generated using LES [11,29,30].

Realistic simulations of spray would describe how a continuous Eulerian liquid phase inside the INCS is pushed through a narrow orifice and break up into a scatter of discrete Lagrangian droplets. However, due to the large separation in physical scales, droplets of a few micrometers compared to centimeters of the liquid column in the INCS, make a full Eulerian description impractical. Instead, this study is limited by the assumption that particles ejected from the INCS are already in an atomized state with a specified particle size distribution. This assumed discrete spherical particles with negligible rotational influence, and negligible particle–particle interaction. The benefit was that no explicit primary atomization was needed to account for the complex physics inside the nozzle where continuous liquid break-up into droplets. In general, near the nozzle of the INCS there is a small volume space with significant interaction of continuous phase and dispersed phase. This area with densely packed particles where the effect of interparticle interaction is important could be treated with additional contact forces, which enter the Lagrangian momentum equations.

5 Conclusions

In conclusion, a computational model for nasal drug delivery using different intranasal corticosteroid sprays for the treatment of Eustachian tube dysfunction was developed. The numerical simulations assessed the particle deposition efficiency on the ET considering the effects of intra- and intersubject variations, spraying in either nostril side, insertion depth, insertion angle, inspiration rates, wall impingement treatment, and fluid film. The main findings are:

(I) Particle deposition efficiency on the ET is less sensitive with Sensimist to intra- and inter-subject anatomy and variations in insertion angle.

(II) Particle deposition efficiency on the ET is more sensitive with Flonase to intra-subject variation in the nasal anatomy and insertion angles.
(III) Both INCS show increased particle deposition efficiency on the ET when including additional outcomes rebound and splash effects in the wall impingement model, whereas fluid film shows an insignificant effect.
(IV) INCS with larger droplet sizes and an insertional angle roughly parallel with the hard palate may yield a more effective particle deposition on the ET.

Funding Data

- NIH (Grant No. K25DC014755; Funder ID: 10.13039/100000002).

Conflict of Interest

There are no conflicts of interest.

References

[1] Shan, A., Ward, B. K., Goman, A. M., Betz, J. F., Reed, N. S., Poe, D. S., and Nieman, C. L., 2019, "Prevalence of Eustachian Tube Dysfunction in Adults in the United States," JAMA Otolaryngol. Head Neck Surg., **145**(10), p. 974.
[2] Aggarwal, R., Cardozo, A., and Homer, J. J., 2004, "The Assessment of Topical Nasal Drug Distribution," Clin. Otolaryngol. Allied Sci., **29**(3), pp. 201–205.
[3] Liu, Y., Matida, E. A., Gu, J., and Johnson, M. R., 2007, "Numerical Simulation of Aerosol Deposition in a 3-D Human Nasal Cavity Using RANS, RANS/EIM, and LES," J. Aerosol Sci., **38**(7), pp. 683–700.
[4] Xi, J., Kim, J., and Si, X. A., 2016, "Effects of Nostril Orientation on Airflow Dynamics, Heat Exchange, and Particle Depositions in Human Noses," Eur. J. Mech. B/Fluids, **55**, pp. 215–228.
[5] Kleven, M., Melaaen, M. C., Reimers, M., Røtnes, J. S., Aurdal, L., and Djupesland, P. G., 2005, "Using Computational Fluid Dynamics (CFD) to Improve the Bi-Directional Nasal Drug Delivery Concept," Food Bioprod. Process., **83**(2), pp. 107–117.
[6] Kimbell, J. S., Segal, R. A., Asgharian, B., Wong, B. A., Schroeter, J. D., Southall, J. P., Dickens, C. J., Brace, G., and Miller, F. J., 2007, "Characterization of Deposition From Nasal Spray Devices Using a Computational Fluid Dynamics Model of the Human Nasal Passages," J. Aerosol Med., **20**(1), pp. 59–74.
[7] Matida, E. A., Finlay, W. H., Lange, C. F., and Grgic, B., 2004, "Improved Numerical Simulation of Aerosol Deposition in an Idealized Mouth–Throat," J. Aerosol Sci., **35**(1), pp. 1–19.
[8] Ferziger, J. H., and Perić, M., 1996, *Computational Methods for Fluid Dynamics*, Springer, Berlin Heidelberg, Berlin, Heidelberg, Germany.
[9] Pope, S. B., 2001, *Turbulent Flows*, Cambridge University Press, New York.
[10] Li, C., Jiang, J., Dong, H., and Zhao, K., 2017, "Computational Modeling and Validation of Human Nasal Airflow Under Various Breathing Conditions," J. Biomech., **64**, pp. 59–68.
[11] Calmet, H., Inthavong, K., Eguzkitza, B., Lehmkuhl, O., Houzeaux, G., and Vázquez, M., 2019, "Nasal Sprayed Particle Deposition in a Human Nasal Cavity Under Different Inhalation Conditions," PLoS One, **14**(9), p. e0221330.
[12] Si, X. A., Sami, M., and Xi, J., 2021, "Liquid Film Translocation Significantly Enhances Nasal Spray Delivery to Olfactory Region: A Numerical Simulation Study," Pharm., **13**(6), p. 903.
[13] Bai, C. X., Rusche, H., and Gosman, A. D., 2002, "Modeling of Gasoline Spray Impingement," Atom. Sprays, **12**(1–3), pp. 1–28.
[14] Fedorov, A., Beichel, R., Kalpathy-Cramer, J., Finet, J., Fillion-Robin, J. C., Pujol, S., Bauer, C., Jennings, D., Fennessy, F., Sonka, M., Buatti, J., Aylward, S., Miller, J. V., Pieper, S., and Kikinis, R., 2012, "3D Slicer as an Image Computing Platform for the Quantitative Imaging Network," Magn. Resonan. Imag., **30**(9), pp. 1323–41.
[15] Mead, J., and Whittenberger, J. L., 1953, "Physical Properties of Human Lungs Measured During Spontaneous Respiration," J. Appl. Physiol., **5**(12), pp. 779–796.
[16] Sundström, E., and Oren, L., 2019, "Pharyngeal Flow Simulations During Sibilant Sound in a Patient-Specific Model With Velopharyngeal Insufficiency," J. Acoust. Soc. Am., **145**(5), pp. 3137–3145.
[17] Sundström, E., Boyce, S., and Oren, L., 2020, "Effects of Velopharyngeal Openings on Flow Characteristics of Nasal Emission," Biomech. Model. Mechanobiol., **19**(5), pp. 1447–1413.
[18] Menter, F. R., 1994, "Two-Equation Eddy-Viscosity Turbulence Models for Engineering Applications," AIAA J., **32**(8), pp. 1598–1605.
[19] Crowe, C. T., Schwarzkopf, J. D., Sommerfeld, M., and Tsuji, Y., 2011, *Multiphase Flows With Droplets and Particles*, CRC Press, Boca Raton, FL.
[20] Ranz, W., and Marshall, W., 1952, "Evaporation From Drops. Parts I & II," Chem. Eng. Progr., **48**, pp. 141–146.
[21] O'Rourke, P. J., and Amsden, A. A., 1987, "The Tab Method for Numerical Calculation of Spray Droplet Breakup," SAE Paper No. 872089.
[22] Hosseini, S., Wei, X., Wilkins, J. V., Fergusson, C. P., Mohammadi, R., Vorona, G., and Golshahi, L., 2019, "In Vitro Measurement of Regional Nasal Drug Delivery With Flonase,® Flonase® Sensimist,™ and MAD Nasal™ in Anatomically Correct Nasal Airway Replicas of Pediatric and Adult Human Subjects," J. Aerosol Med. Pulm. Drug Deliv., **32**(6), pp. 374–385.
[23] Kelly, J. T., Asgharian, B., Kimbell, J. S., and Wong, B. A., 2004, "Particle Deposition in Human Nasal Airway Replicas Manufactured by Different Methods. Part I: Inertial Regime Particles," Aerosol Sci. Technol., **38**(11), pp. 1063–1071.
[24] Zubair, M., 2012, "Review: A Critical Overview of Limitations of Cfd Modeling in Nasal Airflow," J. Med. Biol. Eng., **32**(2), p. 77.
[25] Senecal, P., Schmidt, D., Nouar, I., Rutland, C., Reitz, R., and Corradini, M., 1999, "Modeling High-Speed Viscous Liquid Sheet Atomization," Int. J. Multiphase Flow, **25**(6–7), pp. 1073–1097.
[26] Reitz, R. D., and Diwakar, R., 1986, "Effect of Drop Breakup on Fuel Sprays," SAE Paper No. 860469.
[27] Stiesch, G., 2003, *Modeling Engine Spray and Combustion Processes*, Springer, Berlin/Heidelberg, Germany.
[28] Huh, K. Y., Lee, E., and Koo, J., 1998, "Diesel Spray Atomization Model Considering Nozzle Exit Turbulence Conditions," Atom. Sprays, **8**(4), pp. 453–469.
[29] Sundström, E., and Oren, L., 2019, "Sound Production Mechanisms of Audible Nasal Emission During the Sibilant/S," J. Acoust. Soc. Am., **146**(6), pp. 4199–4210.
[30] Sundström, E., and Oren, L., 2021, "Change in Aeroacoustic Sound Mechanism During Sibilant Sound With Different Velopharyngeal Opening Sizes," Med. Biol. Eng. Comput., **59**(4), pp. 937–945.